Volume 52 | Number 2 | 7 January 2016 | Pages 217–420

ChemComm

Chemical Communications

www.rsc.org/chemcomm

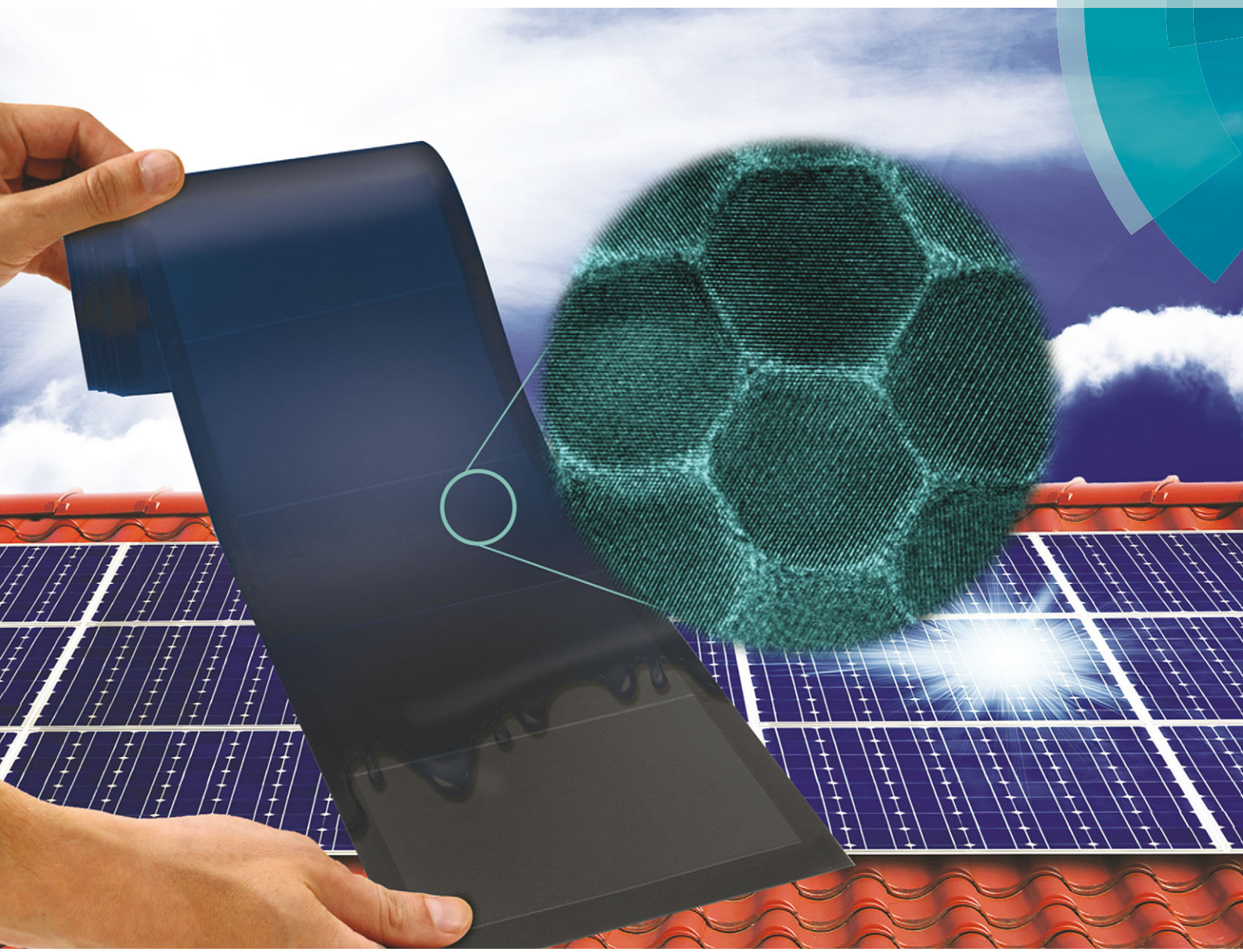

ISSN 1359-7345

ROYAL SOCIETY OF CHEMISTRY

COMMUNICATION

Soubantika Palchoudhury, Karthik Ramasamy, Arunava Gupta *et al.*

A new family of wurtzite-phase Cu_2ZnAS_{4-x} and $CuZn_2AS_4$ (A = Al, Ga, In) nanocrystals for solar energy conversion applications

175 YEARS

ChemComm

COMMUNICATION

View Article Online
View Journal | View Issue

Cite this: *Chem. Commun.*, 2016, 52, 264

Received 15th September 2015,
Accepted 2nd October 2015

DOI: 10.1039/c5cc07743e

www.rsc.org/chemcomm

A new family of wurtzite-phase Cu_2ZnAS_{4-x} and $CuZn_2AS_4$ (A = Al, Ga, In) nanocrystals for solar energy conversion applications†

Anima Ghosh,[ab] Soubantika Palchoudhury,*[a] Rajalingam Thangavel,[b] Ziyou Zhou,[a] Nariman Naghibolashrafi,[a] Karthik Ramasamy*[c] and Arunava Gupta*[a]

A new family of quaternary semiconductors Cu_2ZnAS_{4-x} and $CuZn_2AS_4$ (A = Al, Ga, In) has been synthesized in the form of wurtzite phase nanocrystals for the first time. The nanocrystals can be converted to the stannite phase *via* thermal annealing under a N_2 atmosphere. A direct band gap in the visible wavelength region combined with a high absorption cross-section makes these materials promising for solar energy conversion applications.

The relentless demand in energy generation through non-fossil fuels inspires the scientific community to develop stable and better performing materials that are composed of sustainable, non-toxic and cost-effective elements.[1,2] In this regard, direct band gap I–III–VI_2 based ternary semiconductors are a viable alternative to widely used silicon for photovoltaics since they absorb solar radiation more effectively. Energy conversion efficiencies of nearly 20% have been achieved from I–III–VI_2 based thin film solar cells.[3,4] Despite I–III–VI_2 based materials being more cost-effective and showcasing tremendous potential in efficiency improvement, the cost of energy generation is yet to meet grid parity. This has in large part been attributed to the scarcity of indium. Consequently, significant effort has been devoted to the identification of affordable and sustainable alternatives.[5–9] In recent years Cu_2ZnSnS_4 (CZTS), derived by substituting In with abundant Zn and Sn, has been explored as an alternative with significant progress being already realized.[10–13] Nevertheless, the energy conversion efficiency of solar cells using CZTS still lags behind that for I–III–VI_2 and has not seen an improvement of over 12% in recent years.[14] At this juncture, the quest for affordable and sustainable energy generation materials still remains.[9,15–17] A possible approach to addressing this issue without sacrificing energy conversion efficiency would be to partially substitute In with Zn.[18] Aiming towards this objective, we have for the first time developed a new family of quaternary semiconductors Cu_2ZnAS_{4-x} and $CuZn_2AS_4$ (A = Al, Ga, In) in the form of nanocrystals (NCs). To the best of our knowledge, homogeneous compositions of Cu_2ZnAS_{4-x} and $CuZn_2AS_4$ (A = Al, Ga, In) have not been synthesized previously in any form. Thus far, the closest compositions reported in the literature are for Cu–In–Zn–S wurtzite alloys that are created by alloying different proportions of wurtzite phase $CuInS_2$ and ZnS.[19–23] This method of alloying shifts the band gap of the material beyond the useful solar absorption region and thereby diminishes their suitability for solar cells.[24] Moreover, the Ga and Al analogues of these alloys have not been reported.

Herein we report the synthesis of Cu_2ZnAS_{4-x} and $CuZn_2AS_4$ (A = Al, Ga, In) semiconductors in the form of wurtzite phase NCs along with detailed electronic structure calculations. The band gap of these newly developed materials is in the visible range, between 1.20 and 1.72 eV, meeting the primary requisite for solar cells. Band structure calculations predict direct band gap characteristics for these quaternary semiconductors with high absorption co-efficients and band gaps closely matching with the experimental values. In addition, we show that the NCs can be readily transformed by annealing from the disordered wurtzite phase to the ordered stannite phase without significantly altering their morphologies and optical properties.

The quaternary composition chalcogenide NCs were synthesized using the colloidal hot-injection method.[7] For the synthesis of Cu_2ZnInS_{4-x} (CZIS1) NCs, a 2 : 1 : 1 ratio of acetylacetonate complexes of copper(II), zinc(II) and indium(III) were first heated to 150 °C in oleylamine (OLA) in an inert atmosphere. This was followed by rapid injection of a mixture of *n*-dodecanethiol (*n*-DDT, 1 mL) and *tert*-dodecanethiol (*t*-DDT, 1 mL) and consequent heating of the solution to 250 °C and maintaining at this temperature for 1 h. The mixture was then cooled and cleaned *via* two washes in hexane/ethanol to obtain the final NC product.

[a] *Center for Materials for Information Technology, The University of Alabama, Tuscaloosa, AL, USA. E-mail: agupta@mint.ua.edu, soubantika@gmail.com; Fax: +1-2053482346; Tel: +1-2053483822*

[b] *Department of Applied Physics, Indian School of Mines, Dhanbad, Jharkhand, India. E-mail: thangavel.r.ap@ismdhanbad.ac.in*

[c] *Center for Integrated Nanotechnologies, Los Alamos National Laboratory, Albuquerque, NM, USA. E-mail: kramasamy@lanl.gov*

† Electronic supplementary information (ESI) available: Experimental and theoretical data; SEM, STEM, & EDX: Cu_2ZnInS_{4-x} NCs; TEM & HRTEM of CZAS NCs; XRD: binary phases; summary table for structural and optical properties; XRD: $CuZn_2AS_4$ NCs; Rietveld: Cu_2ZnGaS_{4-x} NCs; XPS: Cu_2ZnInS_{4-x} NCs; and band gap plots: Cu_2ZnAS_{4-x}. See DOI: 10.1039/c5cc07743e

The resulting NCs were readily dispersible in nonpolar solvents like hexane. A similar procedure was used for obtaining the $CuZn_2InS_4$ (CZIS2) NCs, but by changing the metal precursor mixture composition to 1 : 2 : 1 (Cu : Zn : In). The processes for CZIS1 and CZIS2 NCs were extended for synthesizing the analogous Ga and Al compounds using the respective acetylacetonate precursors. The details of the synthesis methods are provided in the ESI.†

The one-step approach described above yields uniform Cu_2ZnInS_{4-x} (CZIS1) nanorods of size ~55 (*l*) × 10 (*w*) nm (Fig. 1a). A similar nanorod morphology has been reported in the literature for a number of other wurtzite phase ternary and quaternary chalcogenide NCs.[9,10,23] The synthesized CZIS1 NCs are highly crystalline (Fig. 1b). Based on the matching of the inter-fringe distances (0.34 ± 0.01 nm) with the (100) plane of wurtzite, the nanorods likely belong to the wurtzite phase (Fig. 1b). To further investigate the compositional homogeneity of the rod-shaped NCs, energy-dispersive X-ray spectroscopy (EDX) measurements have been performed on different regions within the individual NCs using transmission electron microscopy (TEM) and scanning electron microscopy (SEM). The NCs show a homogeneous composition of Cu_2ZnInS_{4-x} (x = 0.5 ± 0.3), closely matching with the stoichiometric ratios (Fig. S1, ESI†). The anion non-stoichiometry seen in these NCs has also been observed for other wurtzite phase chalcogenides, likely to maintain charge neutrality in the compound.[25] Unlike CZIS1, the morphology of $CuZn_2InS_4$ (CZIS2) NCs is quite distinct, being in the form of ~2 μm long and ~27 nm wide nanoworms with slightly curved regions (Fig. 1c). Clear and uniform lattice fringes are also observed in all portions of the worm-like CZIS2 NCs *via* HRTEM indicating a homogeneous composition and high crystallinity (Fig. 1d, Fig. S2 and S3e, f, ESI†). The inter-fringe distance of 0.33 ± 0.02 nm corresponds to the (100) planes of wurtzite.

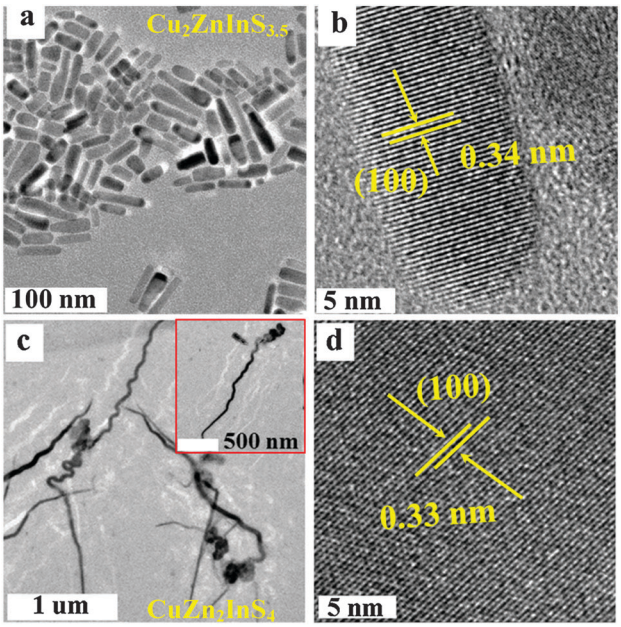

Fig. 1 TEM images of CZIS NCs of different compositions. (a) Cu_2ZnInS_{4-x} (x = 0.5 ± 0.3) nanorods, (b) high resolution TEM (HRTEM) of (a), (c) $CuZn_2InS_{4\pm0.1}$ nanoworms, and (d) HRTEM of (c).

The average chemical composition of the NCs, as determined from the EDX is $CuZn_2InS_{4\pm0.1}$, closely related to the stoichiometric amounts and as expected based on charge neutrality. In the syntheses of CZIS NCs of both compositions, a carefully measured 1 : 1 volume ratio of *n*-DDT and *t*-DDT is essential for stoichiometric and morphological control (Fig. S4, ESI†). The ligand mixture (*n*-DDT and *t*-DDT) serves as the sulfur source and is known to passivate the surfaces to preferentially form wurtzite-phase NC.[26,27]

This robust synthetic technique can be generalized to CZAlS and CZGS, forming a new class of I–II–III–VI chalcogenide NCs (Fig. S5, ESI†). The respective acetylacetonate precursors are particularly chosen for their low decomposition temperature and specific reactivity.[9,28,29] Uniform and nearly spherical NCs of high crystallinity and size ~27 nm can be formed for both Cu_2ZnAlS_{4-x} (x = 0.5 ± 0.3) and $CuZn_2AlS_{4\pm0.1}$ compositions (Fig. S3a and b, ESI†). In contrast, the Cu_2ZnGaS_{4-x} (x = 0.5 ± 0.3) and $CuZn_2GaS_{4\pm0.1}$ NCs of size ~45 nm show a tadpole-like morphology (Fig. S3c and d, ESI†). Interestingly, a somewhat higher reaction temperature (300 °C) is required for these NCs as compared to the CZIS. A possible explanation can be in terms of the difference in the ionic radius since the size of the cation is known to play a key role in the phase and size evolution of NCs.[30] CZAlS and CZGS NCs also exhibit the wurtzite phase, based on the inter-fringe distances.

Phase-pure quaternary Cu_2ZnAS_{4-x} and $CuZn_2AS_4$ NCs have thus far been synthetically challenging to obtain. The primary impediment is the formation of stable binary phases, which should be prevented. Fig. 2a shows powder X-ray diffraction (XRD) measurements confirming the pure wurtzite phases of Cu_2ZnAS_{4-x} NCs. The blue lines indicate the simulated patterns (CaRIne crystallography), considering CZAS as cation-disordered derivatives of the wurtzite ZnS structure, since no standard XRD pattern exists in the database for this family of NCs. XRDa3.1 software is used to match the experimental XRD peaks. These experimental peaks can be indexed to the (100), (002), (101), (102), (110), (103), (200), (112), and (201) planes of pure wurtzite phase [space group *P*63*mc* (No. 186)], in close match with the derived simulated pattern. Based on a comparison of XRD peaks, the NCs are free of any binary phase impurities (Fig. S6, ESI†). The lattice parameter ratio *c*/*a*, as determined from the diffraction peaks is ~1.6, similar to literature reported values for the wurtzite phase of CZTS (Table S1, ESI†). In addition, the pure wurtzite phase is also obtained for the $CuZn_2AS_4$ NC compositions (Fig. S7a, ESI†), leading to a new class of I–II–III–VI wurtzite phase NCs. In general, wurtzite is a cation-disordered metastable phase formed at lower reaction temperatures, while the structurally related ordered stannite/kesterite phases are stable forms at higher temperatures.[24,31,32] To exploit the full potential of our synthetic method, a facile phase transformation approach is investigated for CZAS NCs. The Cu_2ZnAS_{4-x} NCs can be transformed to the pure stannite phase *via* annealing at 400 °C for 2–2.5 h in a N_2 atmosphere, as indicated from the XRD analyses (Fig. 2b).[33] A higher temperature annealing (500 °C) is required for the $CuZn_2AS_4$ NCs (Fig. S7b, ESI†). In addition, Rietveld refinement performed on the experimental XRD pattern shows a

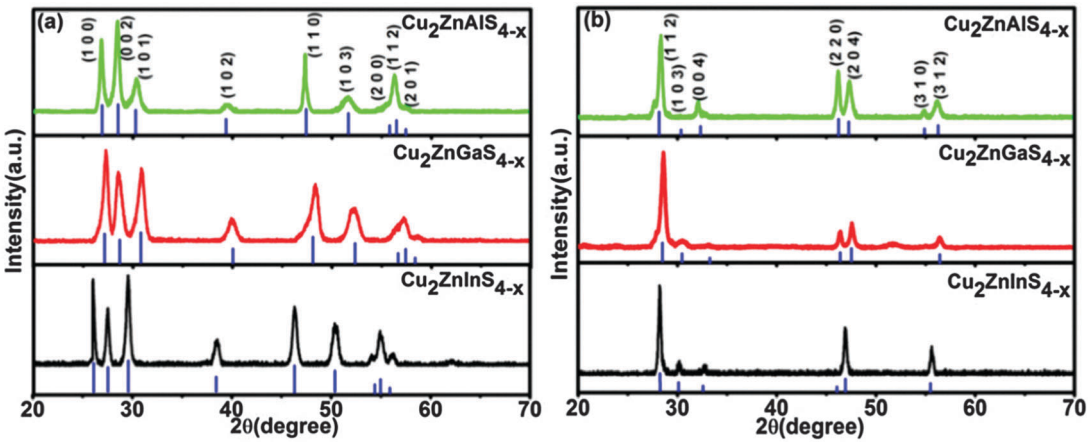

Fig. 2 XRD plots showing the crystal phase of Cu_2ZnAS_{4-x} (x = 0.5 ± 0.3) NCs. (a) Pure wurtzite phase and (b) pure stannite phase after annealing under N_2 atmosphere.

good fit for the wurtzite and stannite phases (Fig. S8, ESI† $CuZn_2AS_{4\pm0.1}$).

X-ray photoelectron spectroscopy (XPS) provides a suitable complement to EDX for chemical composition analysis as it can determine the oxidation states of the constituent elements on the surface of NCs. Fig. S9 (ESI†) shows the representative high resolution XPS pattern for Cu_2ZnInS_{4-x} (x = 0.5 ± 0.3) NCs. The Cu_{2p} core-spectrum shows two major peaks at 931.4 eV ($2p_{3/2}$) and 951.2 eV ($2p_{1/2}$), with a peak splitting of 20.0 eV, indicative of monovalent Cu.[10] The ligand *n*-DDT is likely responsible for the reduction of $Cu(acac)_2$ to Cu(I).[34] Zn_{2p} peaks appear at binding energies 1021.1 eV ($2p_{3/2}$) and 1044.3 eV ($2p_{1/2}$), characteristic of Zn(II) since the peak separation is 22.9 eV (Fig. S9b, ESI†).[10,35] Fig. S9c (ESI†) shows the In_{3d} spectrum with contributions from $3d_{5/2}$ and $3d_{3/2}$ at 444.6 eV and 452.2 eV indicating a spin–orbit splitting of 7.6 eV, characteristic of In(III).[36] The sulfur spectrum with peaks at binding energies 162.2 eV ($2p_{3/2}$) and 163.2 eV ($2p_{1/2}$) and a doublet separation of 1.1 eV can be attributed to the presence of S^{2-} (Fig. S9d, ESI†).[37] The XPS spectrum of $CuZn_2AS_4$ NCs also shows similar oxidation states of the elements.

To investigate the optical properties of the new class of phase-pure wurtzite NCs, ultraviolet-visible spectroscopy (UV-vis) measurements are performed on well-dispersed NC solutions in hexane (Fig. 3a). The direct optical band gaps ($E_{g,opt}$) are determined from the absorbance spectra onset through the extrapolation of the linear portion of the $(A\nu)^2$ *versus* $h\nu$ (A = absorbance, h = Planck's constant, and ν = frequency) plot in the band edge region (Fig. 3b). The band gaps are determined to be 1.78 ± 0.05, 1.64 ± 0.04, and 1.42 ± 0.03 eV for $CuZn_2AlS_{4\pm0.1}$, $CuZn_2GaS_{4\pm0.1}$, and $CuZn_2InS_{4\pm0.1}$, respectively. There is a decrease in the band gap from Al to In, suggesting a likely effect of the increasing ionic radius. Similar band gaps in the visible wavelength range are observed for the Cu_2ZnAS_{4-x} (x = 0.5 ± 0.3) NCs (Fig. S10 and S11, ESI†). For assessing the applicability of these newly developed materials as absorber layers in solar cells, it is important to gain a better understanding of their optical properties. For this purpose we have carried out density functional theory (DFT) calculations using the full-potential linearized augmented plane wave plus local orbital (FP-LAPW+lo) method, as implemented in the WIEN2K code (see the ESI† for details).[38] Our calculations predict a direct band gap transition in both the wurtzite and stannite phases at the Γ point for all $CuZn_2AS_4$ compositions (Fig. 4). The band gap values for the wurtzite phase, estimated from the first principle calculations scissor operator, are 1.71 eV for $CuZn_2AlS_4$, 1.34 eV for $CuZn_2GaS_4$, and 1.26 eV for $CuZn_2InS_4$ (Fig. 3c). These values, along with the decreasing trend from Al to In, are in good agreement with the experimental data. Moreover, the absorption coefficient in the visible wavelength region, which is an important parameter for thin film solar cells, is calculated to be over 10^4 cm^{-1} for these compounds, similar to that for CIGS and CZTS.[7,9,10]

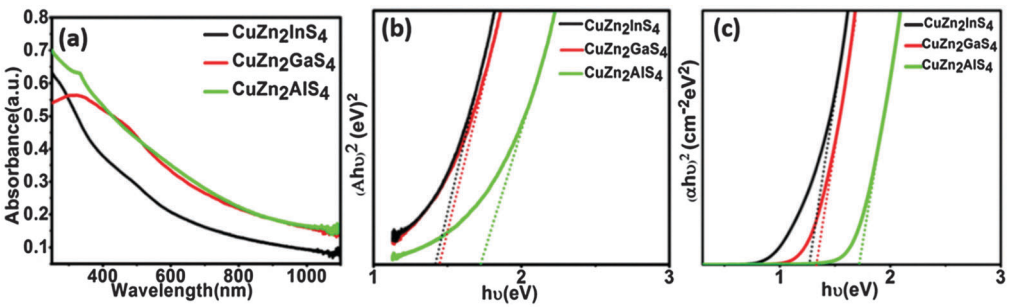

Fig. 3 Band gap measurement of $CuZn_2AS_{4\pm0.1}$ NCs. (a) UV-vis absorption spectra, (b) experimental Tauc plots, and (c) theoretically calculated Tauc plots.

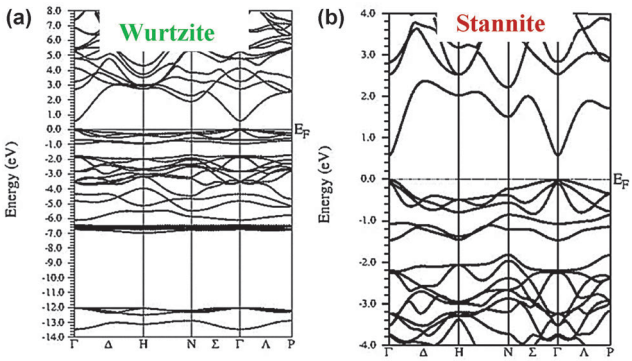

Fig. 4 Band structures of $CuZn_2InS_4$ in (a) wurtzite and (b) stannite crystal phases. Both phases exhibit direct band gap transition with noticeable reduction in carrier mass in the stannite structure. Similar structures have been determined for Al and Ga analogues.

In summary, we have synthesized a new family of quaternary semiconductors Cu_2ZnAS_{4-x} and $CuZn_2AS_4$ (A = Al, Ga, In) in the form of nanocrystals. The NCs are synthesized using the colloidal hot-injection method wherein a mixture of thiols is injected into a vessel containing a solution of the metal precursors at an elevated temperature. We have obtained wurtzite phase NCs with distinct morphologies from nanorods, and nanoworms, to nanotadpoles. These exhibit a homogeneous composition, based on EDX, TEM, and XPS. In addition, phase transformation of the NCs from wurtzite to stannite can be induced *via* annealing under N_2. Importantly, these new compositions are direct band gap materials having band gaps between 1.20 eV and 1.72 eV with a high absorption cross-section, as confirmed from experimental absorption measurements and theoretical calculations. Our initial investigations indicate that these materials possess the requisite optical characteristics to be used as cost-effective and nontoxic absorber layers in solar cell applications. Nevertheless, the full potential can only be confirmed after investigating their charge transport characteristics in solar cell devices, which is being pursued actively in our group and the results will be presented elsewhere.

This work was supported by the US DOE, Office of Basic Energy Sciences, Div. Material Sciences and Eng. Award DE-FG02-08ER46537. A. Ghosh was supported by a Bhaskara Advanced Solar Energy Fellowship of Indo-US Sci & Tech Forum. The authors thank UA-CAF for TEM, SEM, and XPS and UA-Geology Dept. for XRD. The authors thank Rob Holler for XPS measurements. The authors acknowledge UA-MINT and ISM, Dhanbad.

Notes and references

1 D. B. Mitzi, O. Gunawan, T. K. Todorov, K. Wang and S. Guha, *Sol. Energy Mater. Sol. Cells*, 2011, **95**, 1421.
2 S. E. Habas, H. A. S. Platt, M. F. A. M. van Hest and D. S. Ginley, *Chem. Rev.*, 2010, **110**, 6571.
3 T. Saga, *NPG Asia Mater.*, 2010, **2**, 96.
4 L. Li, A. Pandey, D. J. Werder, B. P. Khanal, J. M. Pietryga and V. I. Klimov, *J. Am. Chem. Soc.*, 2011, **133**, 1176.
5 K. Ramasamy, H. Sims, W. H. Butler and A. Gupta, *J. Am. Chem. Soc.*, 2014, **136**, 1587.
6 K. Ramasamy, M. A. Malik, N. Revaprasadu and P. O'Brien, *Chem. Mater.*, 2013, **25**, 3551.
7 X. Zhang, N. Bao, K. Ramasamy, Y. H. A. Wang, Y. Wang, B. Lin and A. Gupta, *Chem. Commun.*, 2012, **48**, 4956.
8 K. Ramasamy, X. Zhang, R. D. Bennett and A. Gupta, *RSC Adv.*, 2013, **3**, 1186.
9 Y.-H. A. Wang, X. Zhang, N. Bao, B. Lin and A. Gupta, *J. Am. Chem. Soc.*, 2011, **133**, 11072.
10 A. Singh, H. Geaney, F. Laffir and K. M. Ryan, *J. Am. Chem. Soc.*, 2012, **134**, 2910.
11 K. Ramasamy, M. A. Malik and P. O'Brien, *Chem. Commun.*, 2012, **48**, 5703.
12 K. Ramasamy, M. A. Malik and P. O'Brien, *Chem. Sci.*, 2011, **2**, 1170.
13 J.-J. Wang, P. Liu and K. M. Ryan, *Chem. Commun.*, 2015, **51**, 13810.
14 J. Kim, H. Hiroi, T. K. Todorov, O. Gunawan, M. Kuwahara, T. Gokmen, D. Nair, M. Hopstaken, B. Shin, Y. S. Lee, W. Wang, H. Sugimoto and D. B. Mitzi, *Adv. Mater.*, 2014, **26**, 7427.
15 N. Guijarro, E. Guillen, T. Lana-Villarreal and R. Gomez, *Phys. Chem. Chem. Phys.*, 2014, **16**, 9115.
16 F.-J. Fan, L. Wu, M. Gong, S. Y. Chen, G. Y. Liu, H.-B. Yao, H.-W. Liang, Y.-X. Wang and S.-H. Yu, *Sci. Rep.*, 2012, **2**, 952.
17 J.-J. Wang, J.-S. Hu, Y.-G. Guo and L.-J. Wan, *NPG Asia Mater.*, 2012, **4**, e2.
18 S. Chen, X. G. Gong, A. Walsh and S.-H. Wei, *Phys. Rev. B*, 2009, **79**, 165211.
19 C. Ye, M. D. Regulacio, S. H. Lim, Q.-H. Xu and M.-Y. Han, *Chem. – Eur. J.*, 2012, **18**, 11258.
20 C. Ye, M. D. Regulacio, S. H. Lim, S. Li, Q.-H. Xu and M.-Y. Han, *Chem. – Eur. J.*, 2015, **21**, 9514.
21 S. Cao, C. Li, L. Wang, M. Shang, G. Wei, J. Zheng and W. Yang, *Sci. Rep.*, 2014, **4**, 7510.
22 L. De Trizio, M. Prato, A. Genovese, A. Casu, M. Povia, R. Simonutti, M. J. P. Alcocer, C. D'Andrea, F. Tassone and L. Manna, *Chem. Mater.*, 2012, **24**, 2400.
23 A. Singh, C. Coughlan, D. J. Milliron and K. M. Ryan, *Chem. Mater.*, 2015, **27**, 1517.
24 R. Mainz, A. Singh, S. Levcenko, M. Klaus, C. Genzel, K. M. Ryan and T. Unold, *Nat. Commun.*, 2014, **5**, 3133.
25 X. Zhang, N. Bao, B. Lin and A. Gupta, *Nanotechnology*, 2013, **24**, 105706.
26 U. Ghorpade, M. Suryawanshi, S. W. Shin, K. Gurav, P. Patil, S. Pawar, C. W. Hong, J. H. Kim and S. Kolekar, *Chem. Commun.*, 2014, **50**, 11258.
27 X. Lu, Z. Zhuang, Q. Peng and Y. Li, *Chem. Commun.*, 2011, **47**, 3141.
28 M. A. Franzman, V. Perez and R. L. Brutchey, *J. Phys. Chem. C*, 2009, **113**, 630.
29 Y. Zou, X. Su and J. Jiang, *J. Am. Chem. Soc.*, 2013, **135**, 18377.
30 F. Wang, Y. Han, C. S. Lim, Y. Lu, J. Wang, J. Xu, H. Chen, C. Zhang, M. Hong and X. Liu, *Nature*, 2010, **463**, 1061.
31 X. Shen, E. A. Hernandez-Pagan, W. Zhou, Y. S. Puzyrev, J.-C. Idrobo, J. E. Macdonald, S. J. Pennycook and S. T. Pantelides, *Nat. Commun.*, 2014, **5**, 5431.
32 S. Chen, A. Walsh, Y. Luo, J.-H. Yang, X. G. Gong and S.-H. Wei, *Phys. Rev. B*, 2010, **82**, 195203.
33 A. Shavel, J. Arbiol and A. Cabot, *J. Am. Chem. Soc.*, 2010, **132**, 4514.
34 J.-J. Wang, D.-J. Xue, Y.-G. Guo, J.-S. Hu and L.-J. Wan, *J. Am. Chem. Soc.*, 2011, **133**, 18558.
35 J. F. Moulder, W. F. Stickle, P. E. Sobol and K. D. Bomben, *Handbook of X-ray photoelectron spectroscopy*, Perkin Elmer, Eden Prairie, MN, 1992.
36 H. Virieux, M. Le Troedec, A. Cros-Gagneux, W.-S. Ojo, F. Delpech, C. Nayral, H. Martinez and B. Chaudret, *J. Am. Chem. Soc.*, 2012, **134**, 19701.
37 V. Lesnyak, C. George, A. Genovese, M. Prato, A. Casu, S. Ayyappan, A. Scarpellini and L. Manna, *ACS Nano*, 2014, **8**, 8407.
38 P. Blaha, K. Schwarz, G. K. H. Madsen, D. Kvasnicka and J. Luitz, *WIEN2k, An Augmented Plane Wave Plus Local Orbitals Program for Calculating Crystal Properties*, Karlheinz Schwarz, Techn. University at Wien, Austria, 2001.